Applied Catalysis B: Environmental 160–161 (2014) 227–239

Contents lists available at ScienceDirect

Applied Catalysis B: Environmental

journal homepage: www.elsevier.com/locate/apcatb

Sunlight assisted photocatalytic mineralization of nitrophenol isomers over W^{6+} impregnated ZnO

A. Hameed[a,c], M. Aslam[a], Iqbal M.I. Ismail[a,b], S. Chandrasekaran[a], M.W. Kadi[b], M.A. Gondal[d,*]

[a] Centre of Excellence in Environmental Studies (CEES), King Abdulaziz University, Jeddah 21589, Saudi Arabia
[b] Department of Chemistry, Faculty of Science, King Abdulaziz University, P.O. Box 80203, Jeddah 21589, Saudi Arabia
[c] National Centre for Physics, Quaid-e-Azam University, Islamabad 44000, Pakistan
[d] Department of Physics, King Fahd University of Petroleum and Minerals, Dhahran 31261, Saudi Arabia

ARTICLE INFO

Article history:
Received 16 November 2013
Received in revised form 7 March 2014
Accepted 8 May 2014
Available online 23 May 2014

Keywords:
Photocatalysis
Nitrophenols
Superoxide radicals
Sunlight
ZnO

ABSTRACT

The synthesis, characterization and sunlight photocatalytic activity of W^{6+} impregnated ZnO for the degradation of nitrophenol isomers (*2-nitrophenol, 3-nitrophenol, and 4-nitrophenol*) is reported. Compared to pure ZnO, the impregnated catalysts exhibited a relatively improved spectral response in the visible region. The significant decrease in luminescence intensity for W^{6+} impregnated catalysts, relative to pure ZnO, established the effective trapping of charge carriers by surface bonded W^{6+} states. The characterization of the impregnated catalysts by FESEM, XRD and XPS revealed the presence of impregnated W^{6+} entities at the surface without affecting the morphology of ZnO. The synthesized catalysts exhibited superior activity for the mineralization of three nitrophenol isomers under sunlight exposure. Based on HPLC analysis, ~99% of *2-* and *4-nitrophenol* was degraded in a short span of 120 min while a degradation of >80% was observed in *3-nitrophenol* in the same period. Time scale TOC measurements ratified the mineralization capability of impregnated catalysts. The release of NO_2^-, NO_3^- ions in the solution, pH measurements and non-existence of hydroxylated aromatic intermediates revealed that superoxide anion radicals ($O_2^{\bullet -}$) are the major contributors in the degradation process. Besides the traces of coupling products, major intermediates identified by GC–MS analysis were either aliphatic dihydroxy alcohols, carboxylic acids or other oxygen containing species depicting that the degradation process proceeds through ring opening mechanism. The W^{6+} impregnated catalyst also furnished high activity in the visible portion of sunlight. Suitable kinetic models were applied to estimate the rate constants (k) of various processes involved in the degradation process. The stability of the photocatalyst against photocorrosion and the possible decrease in the activity of the catalyst in the successive use was also monitored.

1. Introduction

Nitrophenol derivatives, because of their use in a variety of chemical industries, are considered as the major component of the industrial discharge. Being toxic and carcinogenic in nature, the recommended permissible levels of these compounds, especially 2- and 4-nitrophenol in natural water, are less than 10 ppb [1–3]. Nitrophenol derivatives are highly soluble in water and difficult to degrade due to their chemical stability [4,5]. The injurious effects of these compounds demand their priority removal from the water used for human consumption and cultivation. If present in the water, during the chlorination process for disinfection purposes, nitrophenol derivatives are transformed into the secondary stream of more toxic and stable compounds that makes the purification of water after bulk cleaning more difficult and challenging [6]. When present in low concentration, the conversion of toxic aromatic compounds especially phenol derivatives to other more or less toxic compounds further deteriorate the situation [6]. A number of technologies are in use for the removal of nitrophenol derivatives from water streams, however their high operational cost and low efficacy limits the widespread use of these technologies [7–10]. Currently, water purification lacks a single technology capable of removing all the chemical and biological contaminants without leaving any harmful byproducts.

Photocatalysis, being capable of mineralizing the biological and chemical contaminants, is considered as a suitable option in this

* Corresponding author. Tel.: +966 8602351; fax: +966 38602293.
E-mail address: magondal@kfupm.edu.sa (M.A. Gondal).

http://dx.doi.org/10.1016/j.apcatb.2014.05.023
0926-3373/

regard [11–15]. Another attractive choice is the use of sunlight as an excitation source for the mineralization of contaminants. However, the non-availability of the photocatalyst capable of fulfilling the requirements of high photon absorption, stability and photocatalytic activity in the solar spectrum limits the use of this technology. The existing photocatalysts with superior activity, TiO_2 and ZnO, due to their wide bandgap, are able to utilize only 3–5% of the solar spectrum thus restricts the commercial applicability of photocatalysis as a water purification tool. The utilization of sunlight can provide an inexpensive and efficient route for water purification therefore requires the development of photocatalysts with the ability to harvest the maximum portion of the solar spectrum [16–24]. The choices in this contest are either to develop new photocatalysts having activity comparable to TiO_2 or ZnO in sunlight or to modify the existing active photocatalysts by applying suitable surface modifications for better response in sunlight without losing their inherent activity. A number of strategies to enhance the spectral response and the activity of these catalysts are reported in the literature however, no significant breakthrough is achieved in this area [25]. ZnO, being cheap and easily available/synthesizable, is a promising photocatalyst with the activity comparable to TiO_2 [26,27], however, its low spectral response, high luminescence and the abrasion of its outer surface, under illumination, affects its performance with time [28–33].

ZnO is a wide band gap n-type semiconductor (E_g = 3.2 eV) and exists in three possible polymorphs: hexagonal wurtzite, cubic zinc blend, and cubic rock salt [34]. Recently the effect of the shape and size on the photocatalytic activity of nanocrystalline ZnO has been reported [35]. Reports on the photocatalytic activity of polymorphs other than wurtzitic ZnO are scarce.

Surface alteration, especially metal impregnation, is reported as a useful tool for improving both the spectral response and photocatalytic activity of ZnO. The surface presence of the metal not only contributes in suppressing the unwanted recombination of charge carriers but enhance the absorption of photons in the visible region [25,36–38]. The impregnated metal ions, depending on their electronic and chemical nature either alter the band structure of the host photocatalyst or behave independently as the surface photocatalyst [39–45]. The presence of metal ions at the surface protects the surface of ZnO against photocorrosion by engaging the photoexcited electrons.

The photocatalytic degradation of nitrophenol isomer, using TiO_2 and UV light sources of varying intensities, is studied by a number of researchers and reported the successful degradation and transformation of isomers however, most of the studies are limited to experimental results and theoretical estimation of reaction products [46–58]. Only a few studies [46,47] are comprehensive covering most of the details including intermediates identification and proposed reaction mechanism.

The present study is a step ahead for exploring the sunlight active photocatalysts for water purification. Photocatalysis, being limited to surface of the photocatalyst only, the major issues of high electron hole recombination rate and photocorrosion associated with ZnO are addressed by altering its surface with W^{6+} ions. The photocatalytic activity of the impregnated photocatalysts was evaluated for the mineralization of nitrophenol isomers in sunlight exposure and correlated the results obtained by various analytical tools to estimate the nature of oxidizing species involved, the interaction sites and plausible route of degradation and mineralization.

2. Experimental

The W^{6+} impregnated ZnO was synthesized by a two step metal ion impregnation procedure similar to that described for WO_3 in our previous communication [59]. In a representative preparation, ZnO was synthesized by the slow hydrolysis of zinc acetate using KOH as precursor. The obtained gel was washed, dried and powdered before calcinations at 500 °C for five hours in a muffle furnace. For impregnating synthesized ZnO with W^{6+} ions, ammonium meta-tungstate was used as a precursor. Typically, for the synthesis of 1% W^{6+} impregnated ZnO, 0.142 g of ammonium meta-tungstate containing 0.1 g of W^{6+} ions (dissolved in deionized water) was mixed with 10 g ZnO powder obtained in the previous step. The slurry was aged overnight under stirring and dried at 100 °C and heated at 250 °C for the removal of gaseous products such as ammonia. The dried powder were calcined at 500 °C for five hours. The impregnated ZnO catalysts containing 1%, 5%, 10% and 15% W^{6+} ions (w/w) were prepared.

The synthesized powders were analyzed by Perkin Elmer UV-visible diffuse reflectance spectrophotometer for reflectance (%R) and absorption spectra in the solid state. The impact of W^{6+} impregnation on the luminescence behavior of ZnO was studied by HORIBA Scientific, France, Jobin Yvon Fluoro Log 3, macro PL system. The XRD patterns of the pure and W^{6+} impregnated ZnO samples were recorded in the range of 10–80° using Scintag Inc. XDS 2000 diffractometer, USA, equipped with Cu $K\alpha$ source. The identification of existing phases was carried out by matching the main reflections with standard JCPDS cards. High resolution FESEM images of the synthesized powders were acquired by FESEM (JEOL JSM 6490-A, Japan). The XP spectra were recorded by X-ray Photoelectron Spectrometer (PHI 5000 VersaProbe II, ULVAC-PHI Inc., USA) in 0–1100 eV binding energy range.

The photocatalytic degradation of nitrophenol isomers (50 mg L^{-1}) was carried out in the aqueous medium. The 100 ml of photocatalyst/nitrophenol suspension (1 g L^{-1}) was exposed to sunlight in a Pyrex® glass reactor with the diameter of 120 mm and depth of 30 mm without stirring. For comparison, all the experiments were performed in the sunlight intensity of (1000–1100) × 10^2 lx and fixed period of day light in a completely natural environment. The degradation process was monitored by withdrawing a 5 ml sample from the reactor at regular intervals. After removing the photocatalyst by 0.20 μm PTFE WHATMAN syringe filter, the filtered samples were analyzed by Shimadzu UV-1800 spectrophotometer. High performance liquid chromatography (HPLC) analysis of the samples was performed by Shimadzu HPLC, SPD-20A, supplied by Shimadzu Corporation, Japan and equipped with UV detector and c18 column. Methanol–water mixture (60:40) was used as eluent. All the measurements were performed at 254 nm. Thermo scientific, USA, ion chromatograph, Dionex (ICS-5000 + EG Eluent Generator), was used to measure the released ions during the photocatalytic process. Total organic carbon (TOC) of the samples was measured by TOC-V_{CPH} total carbon analyzer supplied by Shimadzu Corporation, Japan. Selected samples were analyzed by GC–MS (Shimadzu Corporation, Japan, Shimadzu-QP 2010 Plus) equipped with a Rtx-1 capillary column, for the identification of unknown compounds formed as intermediate during the mineralization process. Helium (He) was used as carrier gas.

3. Results and discussion

3.1. Characterization

The optical characterization of any synthesized material, especially in photocatalysis, is important as it facilitates the prediction of possible behavior of synthesized photocatalysts under illumination. The major aim of impregnating ZnO with W^{6+} ions was to improve its absorption in the visible region and reduce the extent of undesired recombination of charge carrier for better productivity.

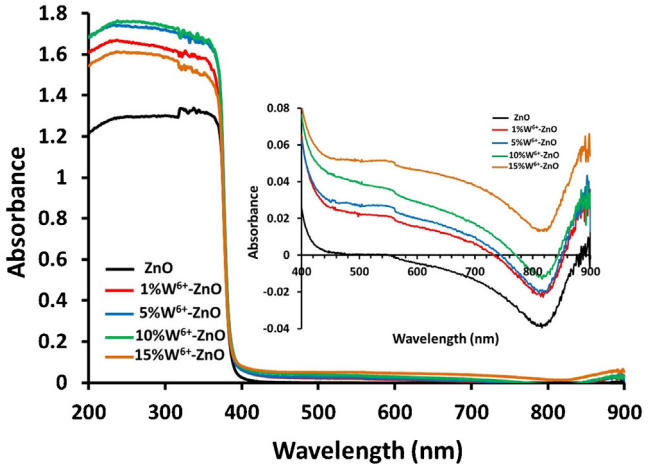

Fig. 1. The comparison of solid-state absorption spectra of bare and W^{6+} impregnated ZnO powders. The onset shows the exploded view of the spectra in 400–900 nm range.

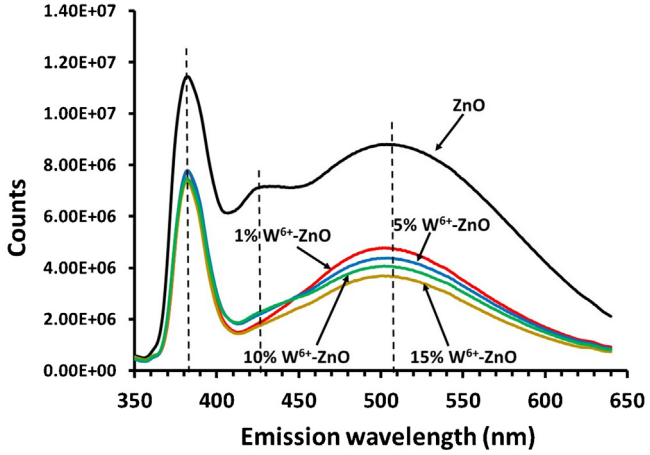

Fig. 3. The comparison of room temperature PL spectra of bare and W^{6+} impregnated ZnO powders at the excitation wavelength of 325 nm by Xenon arc lamp.

The comparison of the absorption spectra of W^{6+} impregnated ZnO powders and bare ZnO support material were recorded in the range of 200–900 nm. As presented in Fig. 1, it is difficult to estimate any visible change in the complete analytical range of 200–900 nm. However, in the exploded view, as shown in the onset of Fig. 1, the improved absorption of photons by the W^{6+} impregnated ZnO photocatalysts, in 400–900 nm (visible region), compared to bare ZnO, can be observed. The absorption increases with the increase in surface density of W^{6+} ions. In pure ZnO, the principal absorption arises due to the excitation of electrons from O (2p) to Zn (3d) orbitals [60]. The shifting of the absorption toward longer wavelengths, red shift, predicts the sharing of singly charged surface O^- by W^{6+} to form surface Zn—O—W type structures on the surface. The enhanced absorption may be a consequence of the alteration of the band structure of ZnO by the impregnated W^{6+} that can cause the lowering of the excitation bandgap. The other possibility is the formation of closely spaced conduction bands corresponding to Zn (3d) and W (5d) by sharing the single valance band O (2p) that, depending on the surface density of W^{6+} states, leads to the probability of photo-excited electron transfer from the valance band O (2p) to the conduction band of both Zn (3d) and W (5d). The diffuse reflectance spectra of the synthesized powders are presented in Fig. 2, where compared to pure ZnO, a decreasing trend in %R for W^{6+} impregnated

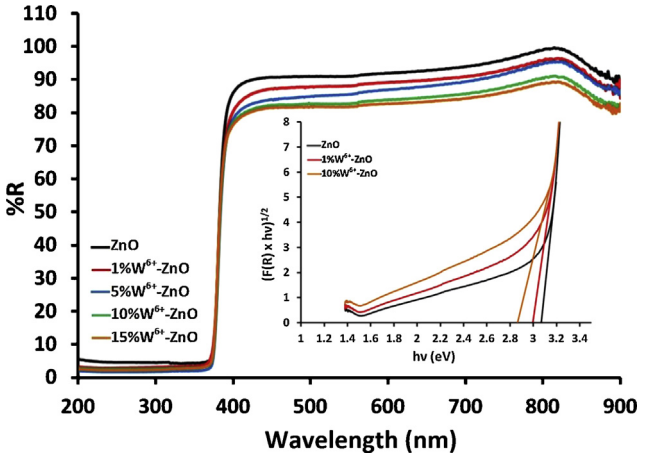

Fig. 2. The comparison of diffuse reflectance spectra of bare and W^{6+} impregnated ZnO powders. The onset shows the graphical determination of bandgap of powders.

samples can be observed. As shown in the offset of Fig. 2, the bandgap of the W^{6+} impregnated powders shifts toward the lower energy with increasing W^{6+} surface states. The successively decreasing bandgap energy with the increasing surface concentration of W^{6+} and the appearance of a single bandgap instead of multiple absorption edges in the impregnated catalysts supports that the impregnation of W^{6+} facilitated the lowering of the bandgap energy of ZnO. Although the presence of W^{6+} ions reduces the O^- generated surface defects however, additional defects in the form of tungsten ions are introduced which serves as sink for photogenerated electrons that cause a significant shift in the absorption edge toward longer wavelengths. The increased extent of *f-f* transitions (t_{2g} to e_g), with the absorption of photons, due to the presence of W^{6+} states, is an additional contributing factor in this regard.

The comparison of room temperature photoluminescence (PL) spectra ($E_{excitation}$ = 325 nm) of bare and W^{6+} impregnated ZnO powders is presented in Fig. 3, where it can be observed that the presence of W^{6+} significantly suppresses the luminescence of ZnO. The decreased luminescence intensity predicts the enhanced suppression of photogenerated charge carrier recombination and augmented lifetime of excited states. For bare ZnO, three emission bands of varying intensity at 382 nm, 429 nm and 505 nm were observed. The strong band at 382 nm corresponds to the bandgap of ZnO. It has been reported that the weak band at 429 nm is due to the interstitial Zn [61]. The broadband at 505 nm corresponds to singly charged oxygen vacancies and its intensity represents the population of O^- defect sites. All the observed values were in accordance with the literature values [60]. A successive decrease in the intensity of the band at 505 nm, representing free O^- sites, was observed with increasing concentration of W^{6+}, which further strengthen the possibility of trapping of electrons by the surface defects induced by W^{6+} states. The closely spaced conduction band of surface WO_6 entities creates these surface defects near the conduction band of ZnO. A ~45% decrease in the intensity of the band at 505 nm was observed for 1% W^{6+}–ZnO. No significant shift in the emission wavelength for synthesized impregnated samples compared to pure ZnO, was observed.

ATR-FTIR analysis of the W^{6+} impregnated samples and pure ZnO, as presented in Fig. 4, was performed to locate the binding site of W^{6+}. The analysis was concentrated on the identification of Zn—O^- bands in bare ZnO and Zn—O—W bands in W^{6+} impregnated samples. The Zn—O^- stretching band in pure ZnO was identified at 597.9 cm^{-1}. With the addition of W^{6+} at the surface of ZnO, an observable change, both in the position and intensity of Zn—O^- band was observed. For 1% W^{6+}-ZnO, the intensity of Zn—O^- band

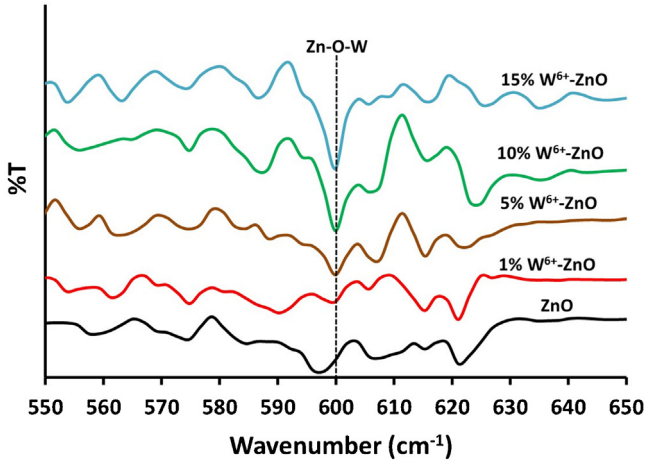

Fig. 4. The ATR-FTIR spectra of bare and W^{6+} impregnated ZnO powders for the identification of Zn–O–W bonds.

at 597.9 cm^{-1} was decreased and another band at 600 cm^{-1} which was identified as Zn—O—W emerged. With the further addition of W^{6+}, the Zn—O^- stretching band completely disappeared while the intensity of the band at 600 cm^{-1} progressively increased. The identification of intense Zn—O—W band further strengthens the assumption of shared surface oxygen between Zn^{2+} and W^{6+}.

The high resolution (120,000×) FESEM images of bare and W^{6+} impregnated ZnO are compared in Fig. 5a–e. It can be noticed that the impregnating W^{6+} ions are homogeneously dispersed on the surface without altering the morphology of hexagonal ZnO rather than being inserted into the lattice causing structural distortion or deformation. Also the absence of aggregates or clusters completely negated the formation of WO_3 as independent entities. The uniform surface distribution, especially for 1% and 5% impregnated samples, revealed that the singly charged surface oxygen serve as the binding link between Zn^{2+} and impregnating W^{6+}. For 10% and 15% impregnated samples (Fig. 5d and e), the diminishing of the sharp margins of hexagonal rod shaped particles indicated the layered deposition of W^{6+} entities.

The XRD patterns of pure hexagonal ZnO in comparison with W^{6+} impregnated samples are presented in Fig. 6a, where it can

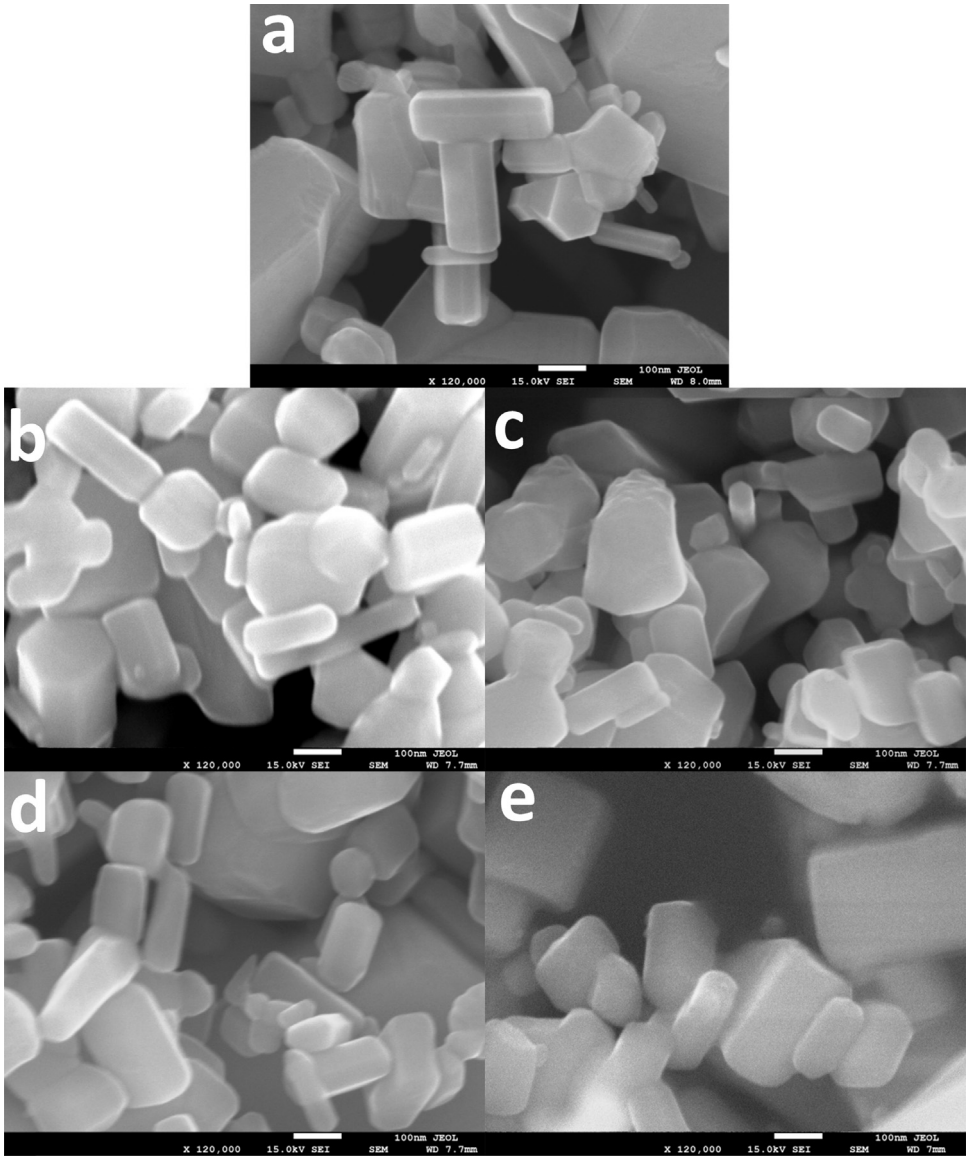

Fig. 5. The comparison of high resolution (120,000×) FESEM images of (a) bare ZnO, (b) 1% W^{6+}–ZnO, (c) 5% W^{6+}–ZnO, (d) 10% W^{6+}–ZnO, (e) 10% W^{6+}–ZnO.

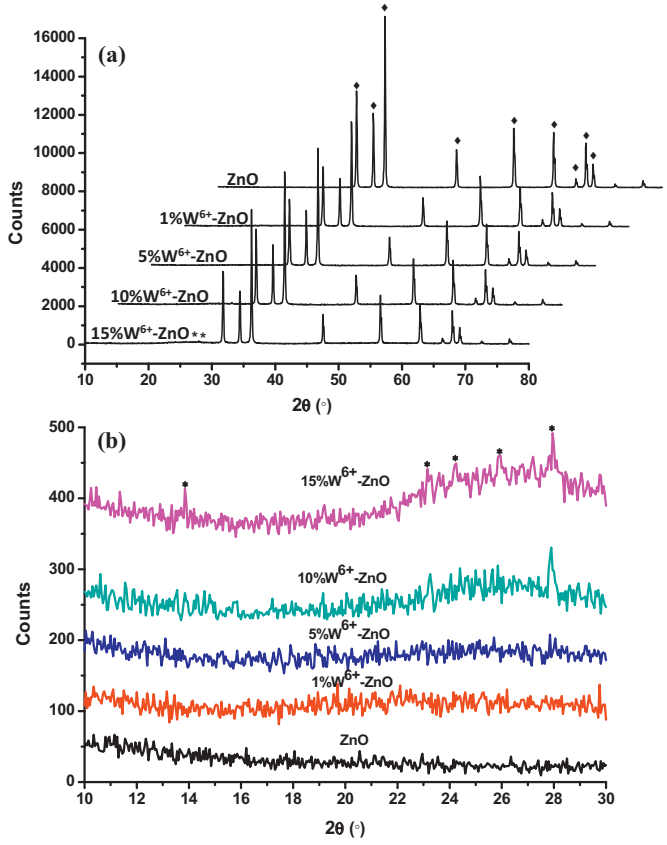

Fig. 6. The comparison of XRD patterns of bare ZnO and W^{6+} impregnated ZnO (a) in $2\theta = 10–80^{\circ}$ range, (b) in $2\theta = 10–30^{\circ}$ range.

be noticed that the reflections due to hexagonal ZnO dominate the XRD patterns however, a decrease in the intensity of the major reflections was observed with the increasing density of W^{6+} states. The peaks identified by (♦) corresponds to (100), (002), (101), (102), (110), (103), (200), (112), (004), and (002) reflections arising from ZnO (JCPDS-36-1415). The similarity in the XRD patterns of pure and W^{6+} impregnated ZnO samples specified that the W^{6+} ions only reside at the surface in the form of Zn—O—W structures without affecting the lattice of ZnO base. The FESEM (Fig. 5) and FTIR analysis (Fig. 4) also support the same finding. With the increasing concentration of W^{6+} ions, the layer by layer deposition leads to the formation of highly dispersed WO_3 microstructures. The appearance of minor peaks in $2\theta = 20–30^{\circ}$ region, for 10% and 15% W^{6+} impregnated samples, as presented in Fig. 6 b, confirmed the formation of surface WO_3 states. The careful identification of these peaks revealed the resemblance of these surface states with that of monoclinic WO_3 (JCPDS-43-1035). These peaks were not observable for lower concentrations of W^{6+} entities. The applications of the Scherrer's equation on the main reflections of all the patterns revealed no significant change in the crystallite size of ZnO support that ranged between 45 and 60 nm.

The comparison of the XPS survey scans (0–1100 eV) of pure, 1% and 10% W^{6+} impregnated ZnO samples is presented in Fig. 7. The appearance of W 4f and W 4d peaks in impregnated samples confirmed the existence of W in the samples. The O 1s peaks of the three samples are compared in Fig. 8a, where a shift in the maximum binding energy can be observed. The deconvolution of the ZnO, O 1s peak revealed two major peaks at 531.6 eV and 532.0 eV, which is in accordance with the literature values [62]. With the increasing concentration of W^{6+} ions at the surface of ZnO, the decrease in O 1s peak intensity along with the shifting of

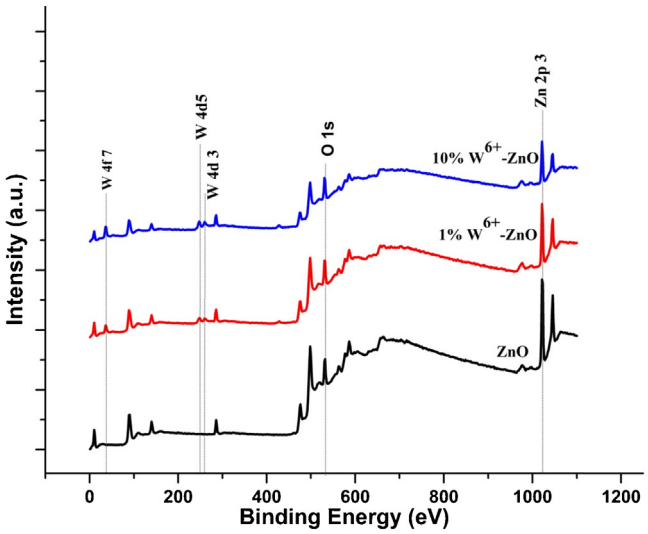

Fig. 7. The comparison of the survey scans of bare, 1% and 10% W^{6+} impregnated ZnO.

maxima to 530.4 eV, attributed to the formation of Zn—O—W structures, was also evidenced. A similar trend was observed for Zn 2p peaks (Fig. 8b) that appeared at 1020.22 eV and 1022.33 eV. The increasing surface coverage by W^{6+} entities shifted the Zn 2p peaks to higher binding energies of 1021.13 eV and 1022.61 eV with decreased intensity. The comparisons of W 4d and W 4f is presented in Fig. 8c and d. W $4d_{5/2}$ and W $4d_{3/2}$ appeared at the binding energies 247.2 eV and 260.0 eV that corresponds to W^{6+} states [63]. The broad peak of W 4f core levels at 36.77 eV for 1% and 37.09 eV for 10% W^{6+} impregnated ZnO (Fig. 8d) corresponds to unresolved W $4f_{7/2}$ and W $4f_{5/2}$ states. The curve fitting for 10% samples revealed a pair of peaks arised due to spin–orbit splitting at 36.29 eV and 37.43 eV confirmed the presence of tungsten as W^{6+} [63].

3.2. Photocatalytic mineralization of nitrophenol isomers

The major reactive oxygen species (ROS), produced because of the creation of photon induced $e^- – h^+$ pair, are hydroxyl ($OH^{\bullet}$) and superoxide anion ($O_2^{\bullet -}$) radicals. The band edge potentials (E_{vb}, E_{cb}) of the semiconductor and pH of the photocatalytic system regulate the generation and population of these species in aqueous system. It is believed that hydroxyl radicals ($OH^{\bullet}$) are instantaneously generated with the absorption of photons having energy equal to or higher than the bandgap of the semiconductor [64]. The superoxide anions ($O_2^{\bullet -}$) are produced due to one electron reduction of oxygen molecules by the conduction band electrons. The O_2 molecules are either already present in the system as dissolved O_2 or produced in situ. The reduction of O_2 by photoexcited electrons (e_{cb}^-) requires the potential of conduction band either at −0.28 V or higher on the negative scale. The process of formation of hydroxyl radicals ($OH^{\bullet}$) and superoxide anions ($O_2^{\bullet -}$) can be represented by Eqs. (1)–(4).

$$SC + h\upsilon \xrightarrow{E>Eg} h_{vb}^{+} + e_{cb}^{-} \quad (1)$$

$$H_2O + h_{vb}^{+} \rightarrow OH^{\bullet} + H^{+} \quad (2)$$

$$OH^{\bullet} + OH^{\bullet} \rightarrow H_2O + {}^{1}/_{2}O_2 \quad (3)$$

$$O_2(\text{Dissolved}) + e_{cb}^{-} \rightarrow O_2^{\bullet -} \quad (4)$$

The hydroxyl radicals ($OH^{\bullet}$) carries free electrons while the superoxide anion ($O_2^{\bullet -}$) radicals bear additional negative charge along with free electrons. Keeping in view the chemical nature of these two oxidizing species, it can be predicted that the degradation process initiated by $OH^{\bullet}$ radicals should progress through the

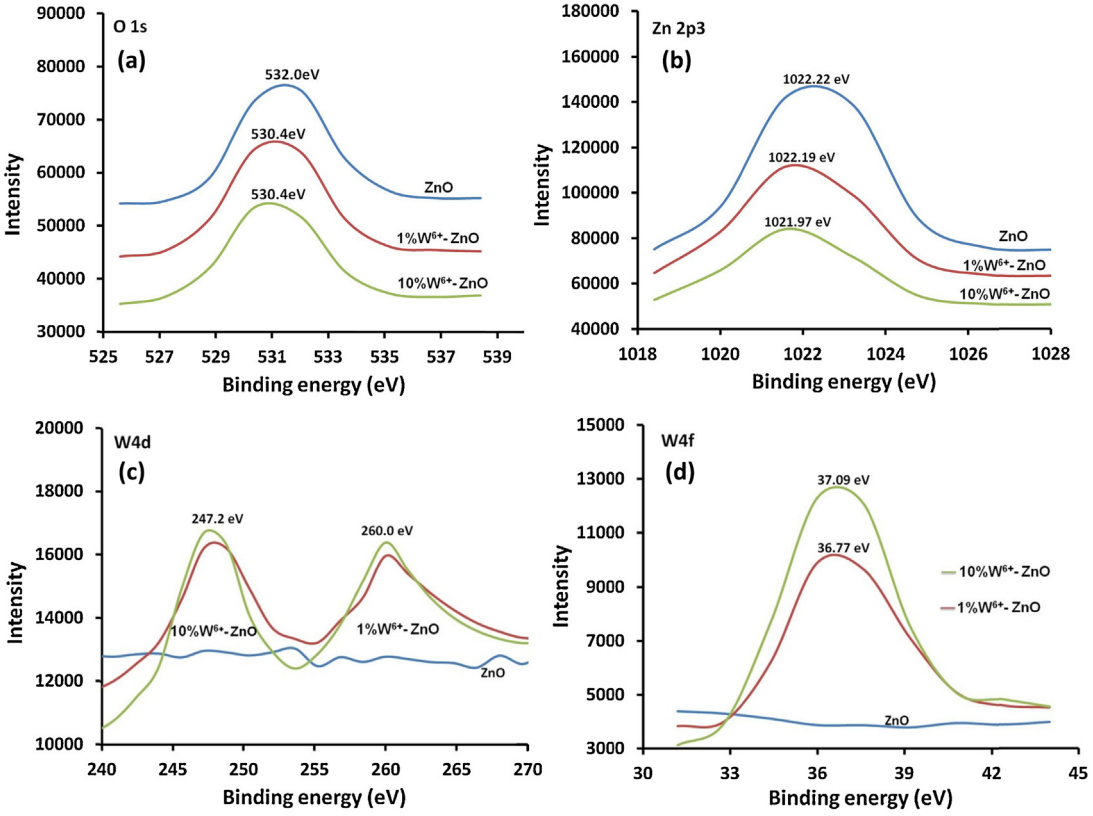

Fig. 8. The comparison of (a) O 1s levels (b) Zn 4p3 levels (c) W 4d splitted levels and (d) W 4f levels in pure, 1%, and 10% W^{6+} impregnated ZnO.

formation of hydroxylated intermediates with fewer ions in the solution similar to free radical reactions. On the other hand, the interaction of $O_2^{\bullet-}$ anions, being charged in nature, should lead to high mineralization without significant hydroxylated intermediates and appreciable proportion of inorganic ions (if present in the organic structure).

As presented in Fig. 9, the absorption bands of 2-NP and 4-NP were shifted immediately after the addition of the photocatalyst in the dark while for 3-NP, no significant shift in the absorption pattern was observed. In the aqueous solution, the K_a values of 2-, 3- and 4-NP at 25 °C are 6×10^{-8}, 5.0×10^{-9} and 6.9×10^{-8} respectively, which predict the low dissociation of 3-NP compared to 2-NP and 4-NP. With the addition of ZnO based catalyst, the presence of singly charged O^- sites on the surface of the ZnO base ($ZnO_{pH_{ZPC}} = 9$), completely de-protonate 2- and 4-NP, creating the resonance stabilized 2- and 4-nitrophenoxy ions in the solution that results in the significant change in absorption spectra. The conjugated bases of 2- and 4-NP are additionally stabilized by the delocalization of the negative charge on the NO_2 group. While the conjugate base of 3-NP i.e. 3-nitrophenoxy ions, lacks the delocalization of the electronic charge to NO_2 group and experience the low magnitude of resonance stabilization in solution thus no significant change in the absorption spectra was spotted. This observation is worth

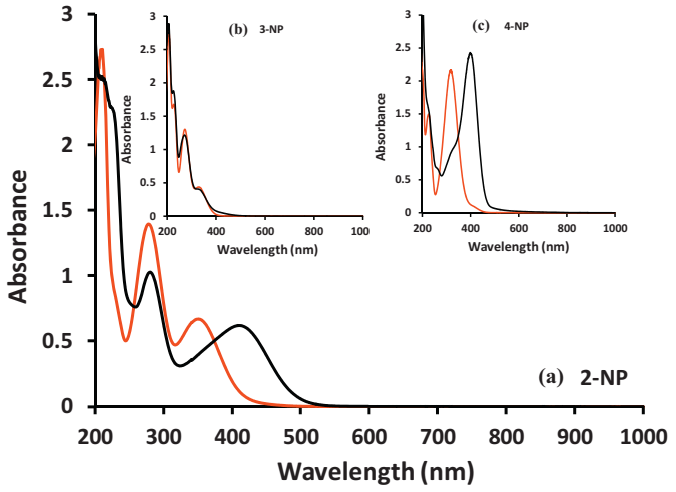

Fig. 9. The variation in the absorption spectra (a) 2-NP (b) 3-NP and (c) 4-NP with the addition of the catalyst in the dark.

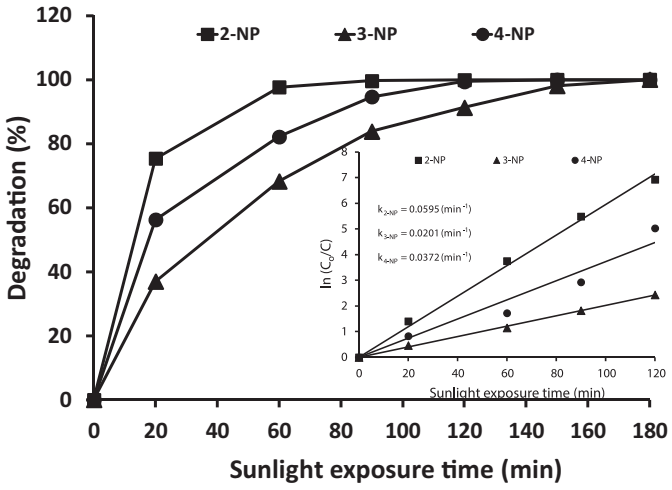

Fig. 10. The degradation profile of 2-NP, 3-NP and 4-NP in the sunlight exposure over 1% W^{6+}–ZnO. The onset shows the evaluation of rate of degradation of nitrophenol isomers.

mentioning here as neglecting the shift in the absorption spectra of nitrophenols may lead to false observation especially in the fixed wavelength experiments. The resonance stabilized structures of the 2-, 3- and 4-nitrophenoxy ions are presented below.

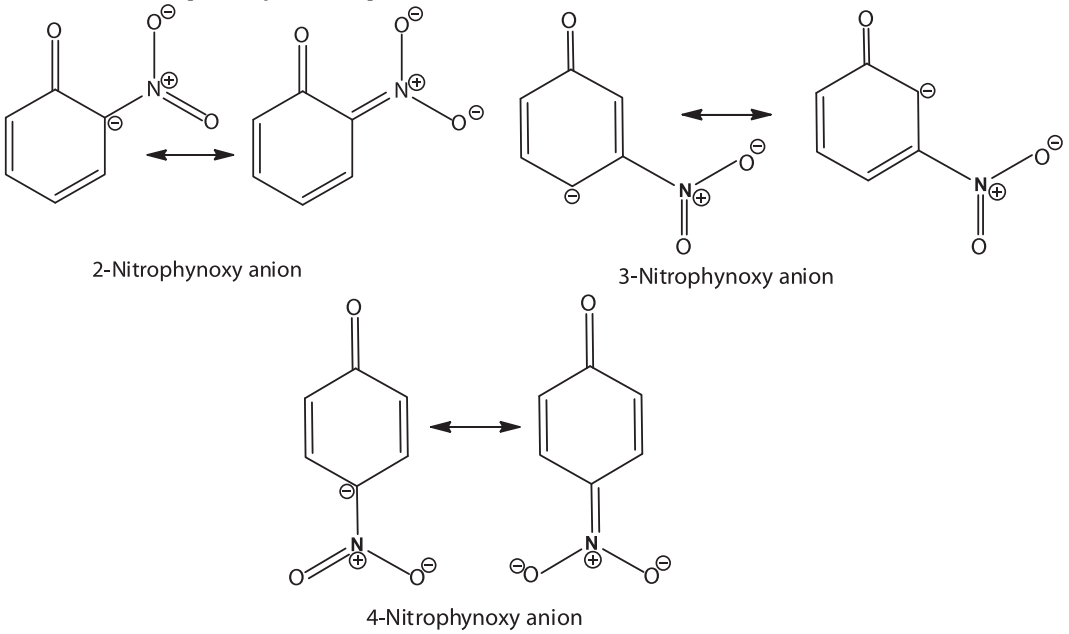

Among all the synthesized catalyst, 1% W^{6+} impregnated ZnO showed the highest activity for the mineralization of nitrophenol isomers therefore, the results obtained for the same catalyst would be discussed in detail. The effect of increasing the W^{6+} loading on the degradation process will be compared later in the discussion. The degradation of nitrophenol isomers was monitored by both UV–visible spectroscopy and high performance liquid chromatography (HPLC). The UV–visible spectroscopy based degradation profiles of nitrophenol isomers, as a function of time, are shown in the supplementary details (Figs. S1–S3). HPLC measurements were found more accurate and reproducible compared to UV–visible spectroscopy since the presence of intermediates, even in the low concentration; influence the absorbance of the substrate under study, resulting in the doubtful absorbance values. Therefore, the mineralization of 2-, 3- and 4-nitrophenol was evaluated based on the decrease in the peak heights of HPLC chromatograms using the following relation.

$$\text{Degradation}\ (\%) = \frac{(C_o - C_t)}{C_o} \times 100 = \frac{(H_o - H_t)}{H_o} \times 100$$

where H_o is the peak height of 50 ppm nitrophenol substrate ($t = 0$) and H_t is the peak height after sunlight exposure for time "t". As presented in Fig. 10, in 90 min of sunlight exposure, compared to the degradation of ≤50% for bare ZnO, a degradation of ~99.7%, ~83.7% and ~94.6% were observed for 2-NP, 3-NP and 4-NP, respectively. Among the three isomers, 2-NP was completely degraded in 90 min while 4- and 3-NP consumed 120 and 180 min respectively, in sunlight exposure for complete removal. These observations are consistent with previous studies [46,47].

The higher activity of W^{6+} impregnated catalyst, compared to bare ZnO, clearly indicate the existence of synergy between the base ZnO and the impregnating metal that facilitates the trapping and productive transfer of electrons to dissolved oxygen for the generation of superoxide anion radicals. It is proposed that the photogenerated electrons from the conduction band of ZnO are transferred to surface W^{6+} entities, which serve as electron capture sites. W^{6+} states accommodate the trapping and transfer of electrons by adjusting the oxidation states to W^{5+} that involves bond rupture and formation as explained in Eqs. (5) and (6).

$$e_{cb}(\text{ZnO}) + W^{6+}O_6(\text{surface}) \rightarrow W^{5+}O_5(\text{surface}) + O^-(\text{surface}) \quad (5)$$

$$W^{5+}O_5(\text{surface}) + O^-(\text{surface}) + O_2(\text{dissolved}) \rightarrow W^{6+}O_6(\text{surface}) + O_2^{\bullet -} \quad (6)$$

The comparison of HPLC chromatograms of the samples drawn at regular intervals for 2-NP, 3-NP and 4-NP is presented in supplementary details (Figs. S4–S6). Noticeably, compared to the extent of decrease in the concentration of respective nitrophenol isomers, a low concentration of intermediates can be observed. Secondly, a fast decreasing trend in the intermediates can also be observed. The sharp decrease in nitrophenol substrates without the formation of significant sums of intermediates suggested that the degradation process proceeds though alternative mechanism other than $OH^{\bullet}$ interaction that leads to complete mineralization directly. This observation was contrary to the previous studies [46,47] where, based on experimental evidences, the $OH^{\bullet}$ were regarded as responsible for the degradation and mineralization of nitrophenols and a variety of hydroxylated aromatic intermediates that included mainly di-hydroxy phenols and their derivatives were identified. Surprisingly, in the present study, no hydroxylated aromatic intermediate was identified by either HPLC or GC–MS analysis. The absence of expected aromatic intermediates that are mandatory with the photocatalytic mineralization through $OH^{\bullet}$ radical attack further strengthened the view that the mineralization process is conceded out by superoxide anion ($O_2^{\bullet -}$) radicals. The possible reaction mechanism in case of $OH^{\bullet}$ and $O_2^{\bullet -}$ radical attack and the nature of intermediates is presented below. The non-existence of hydroxylated aromatic intermediates was further verified by analyzing the mixture of available dihydroxy phenols namely pyrocatechol, resorcinol and hydroquinone, by HPLC (keeping the same analytical conditions) and the results were matched with the

chromatograms of 2-, 3- and 4-NP acquired at different time intervals. No matching was observed in the retention time of intermediates and standard compounds. The comparison is presented in the supplementary details (Fig. S7). This observation led to the conclusion that, as reported recently [65], it is a misconception that hydroxyl radicals ($OH^{\bullet}$) play the major oxidizing role in all the photocatalytic degradation/mineralization processes. The possible formation and contribution of reactive oxygen species (ROS) in the aqueous photocatalytic system can be predicted on the basis of the nature of the photocatalyst, band edge potentials of photocatalyst and intermediates formed during the photocatalytic process. In the present case, the conduction band edge potential of the base material, ZnO (−0.33 eV) and the aliphatic nature of intermediates formed, supports the leading role of superoxide anions ($O_2^{\bullet -}$) radicals however, in the presence of suitable valance band potential of ZnO (+2.89 V), the contribution of hydroxyl radicals cannot be completely negated. The formation and existence of ROS ($OH^{\bullet}$ and $O_2^{\bullet -}$) in an aqueous photocatalytic system are sensitive to the pH of the system [65–67]. The pH changes during the photocatalytic degradation of 2-, 3- and 4-NP is presented in Fig. 11 where it can be observed that the pH remain in the neutral range, which further supports the occurrence of superoxide anions in the system which transforms to $HO_2^{\bullet}$ at pH below 4.8 [66,67]. The initial decrease followed by the sharp increase in pH, for 2-NP, supports the rapid release of NO_2^- ions in the solution. A similar pattern, with a low magnitude can be observed for 3- and 4-NP.

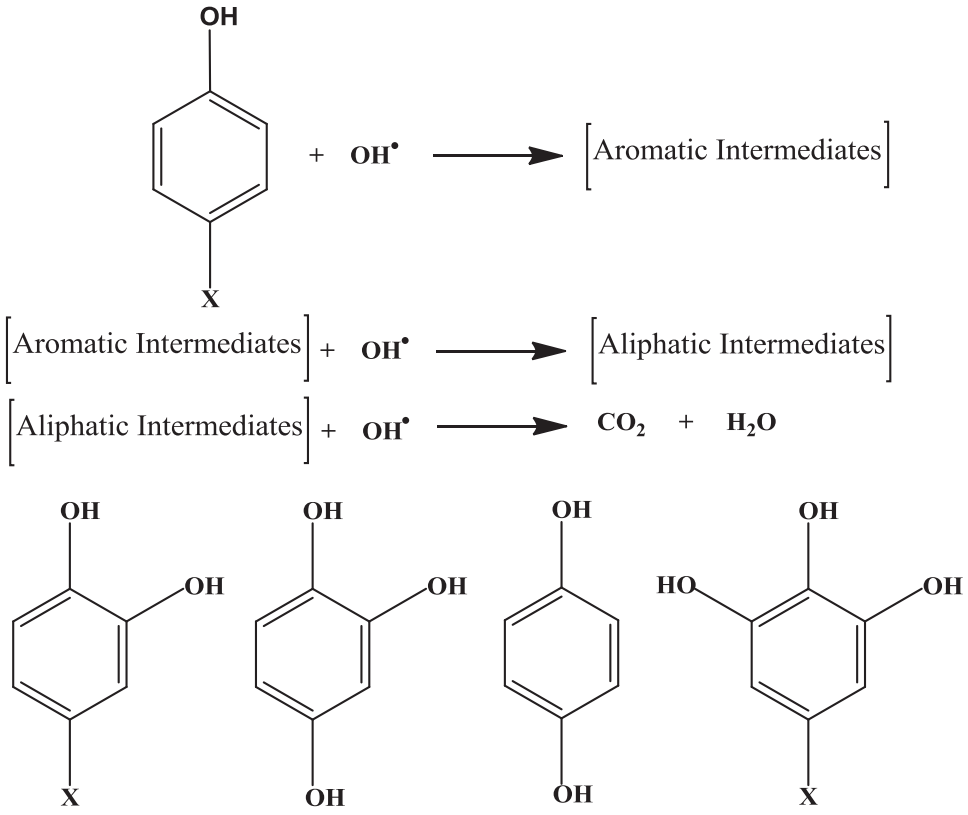

Some of the possible aromatic intermeditaes

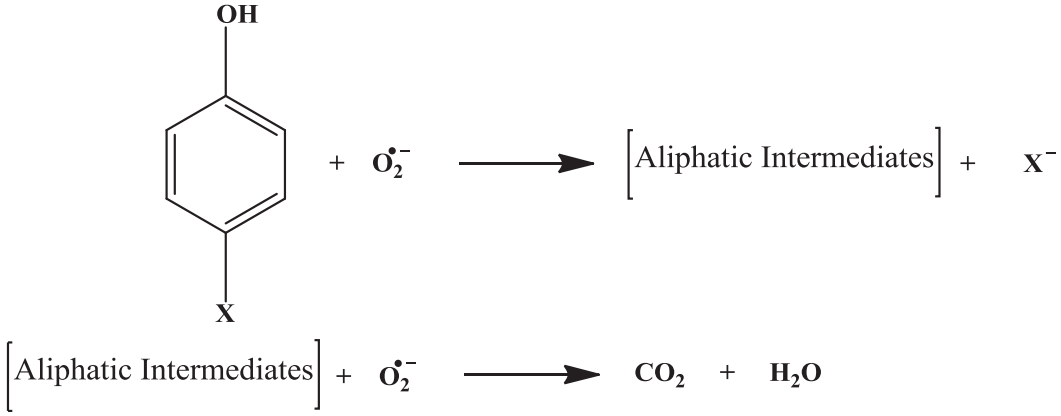

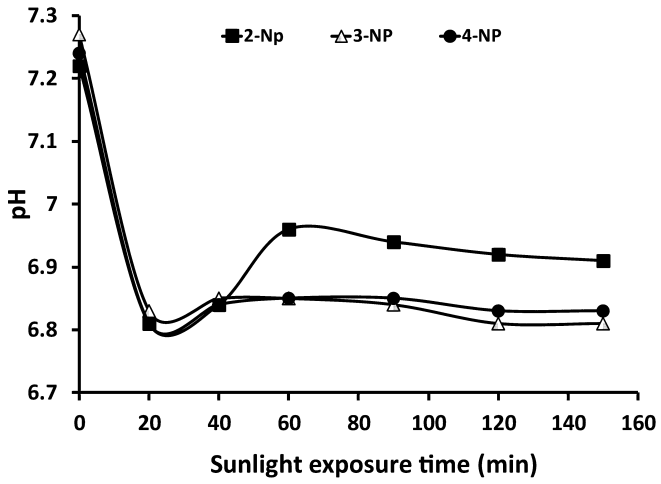

Fig. 11. pH changes during the mineralization of 2-NP, 3-NP and 4-NP in the sunlight exposure over 1% W^{6+}–ZnO.

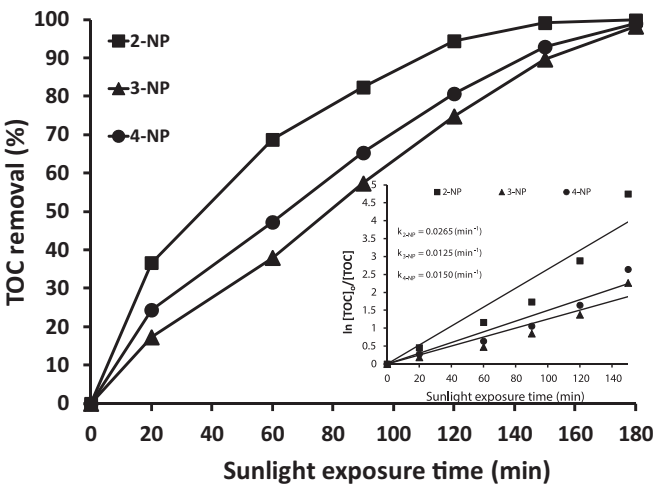

Fig. 12. The TOC removal profile of 2-NP, 3-NP and 4-NP in the sunlight exposure over 1% W^{6+}–ZnO. The onset shows the evaluation of rate of TOC removal of nitrophenol isomers.

The kinetics of the degradation of nitrophenol isomers were evaluated by applying a number of kinetic models. A Langmuir–Hinshelwood model for pseudo first order kinetics was observed to be the best-fit model for optimum correlation. The plot of $\ln(C_o/C_t)$ as a function of sunlight exposure time (t) is presented at the onset of Fig. 10. The rate constant k (min^{-1}) was evaluated by applying the linear regression of the degradation data. The evaluated rate constants for the three isomers the order:

$k_{2\text{-NP}} > k_{4\text{-NP}} > k_{3\text{-NP}}$.

The total organic carbon (TOC) removal efficiency actually establishes the true mineralization credibility of a photocatalyst. The time scale TOC removal of the three isomers is presented in Fig. 12. The relatively slow rate of TOC removal, compared to the overall degradation of 2-, 3- and 4-NP, confirmed that the three isomers through intermediate formation. The evaluation of the rate of TOC removal for the three isomers is presented at the onset of Fig. 12. For 2-NP, compared to almost complete removal of nitrophenol substrate in 90 min of sunlight exposure, ~99.99% removal of TOC was accomplished in 180 min of sunlight exposure with a rate of 0.0265 min^{-1}. For 3- and 4-NP, in the same period, ~98.48% and 98.96% of TOC was removed with a rate of 0.0125 min^{-1} and 0.0150 min^{-1} respectively. By comparing the degradation and TOC removal curves for the three isomers, it can be inferred that $O_2^{\bullet-}$ anions interact simultaneously with the nitrophenol substrates and intermediates formed. Initially in the absence of intermediates, the majority of $O_2^{\bullet-}$ anions is consumed in the degradation of nitrophenol substrates (the observed high degradation of the three isomers in the first 20 min). The formation of intermediates affects the degradation of nitrophenol isomers as a significant proportion of generated $O_2^{\bullet-}$ anions is engaged in intermediate mineralization.

The comparison of the release of NO_2^- and NO_3^- ions, during the course of the photocatalytic degradation process for 2-, 3-, and 4-NP is presented in Fig. 13a–c respectively, where it can be observed that the release of NO_2^- ions follow the similar pattern as that of degradation of respective nitrophenol isomer. The release of negatively charged NO_2^- ions in the solution, with the degradation of nitrophenol substrates, also supports the involvement of negatively charged superoxide ions in the degradation process. The presence of electron withdrawing NO_2 groups in nitrophenols activates the sites of attack for the incoming radicals or ions [4], as presented below.

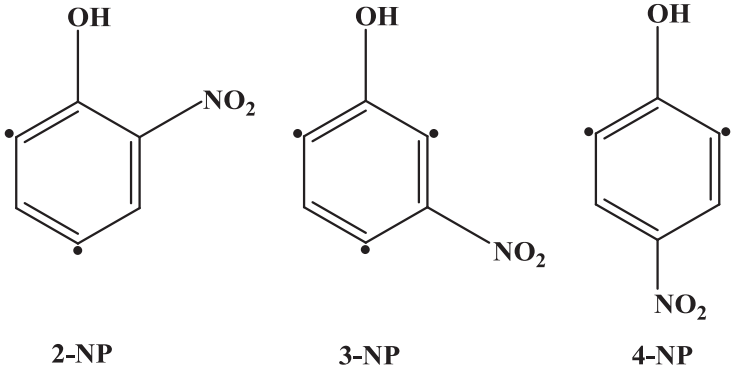

It can be inferred that if $O_2^{\bullet-}$ anions attacks the sites which are activated by the presence of the NO_2 group on the ring, the NO_2 bearing open chain compounds should be identified as intermediates. In addition, the rate of release of NO_2^- ions should be significantly lower compared to that observed. The observations contrary to the above mentioned assumptions led to the conclusion that superoxide anions are highly selective in their attack. Being charged in nature, attack on the NO_2 binding carbon atom which causes the cleavage of aromatic structure and release of NO_2^- ions. The variation in the rate of release of NO_2^- ions in the solution for three isomers is likely to be dependent on the position, orientation, steric hindrance and stability induced by resonance and inductive effects. The favorable orientation of NO_2 groups in 2-NP makes it a soft target for $O_2^{\bullet-}$ anions attack thus causing the efficient degradation and release of NO_2^- ions in the solution. The additional inductive effect in 4-NP makes it difficult for $O_2^{\bullet-}$ anions to displace NO_2 groups thus a relatively lower rate of NO_2^- release is

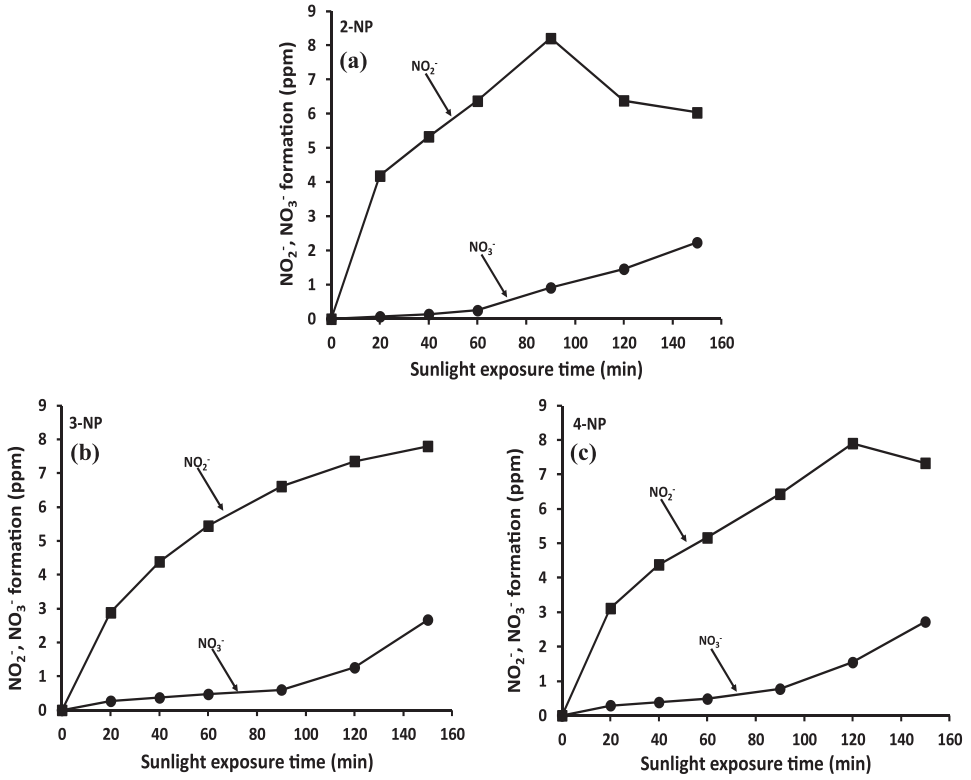

Fig. 13. NO_2^-, NO_3^- profile of nitrophenol isomers in the sunlight exposure over 1% W^{6+}–ZnO. (a) 2-NP, (b) 3-NP, (c) 4-NP.

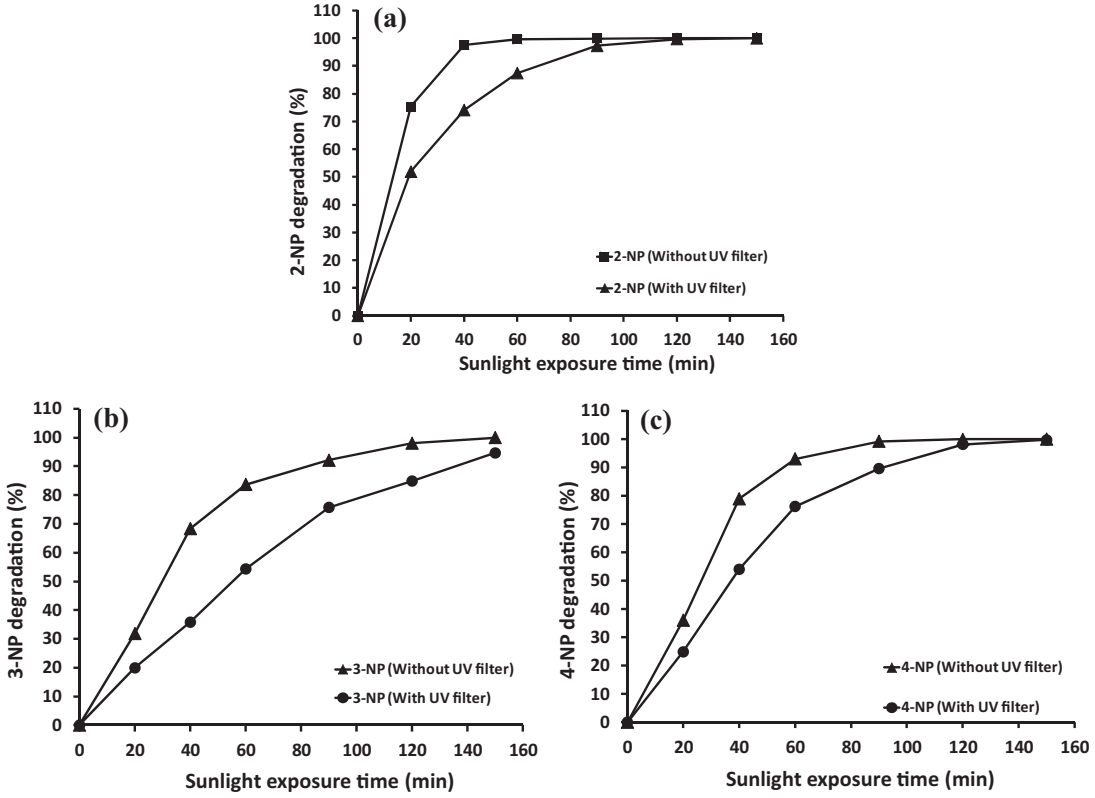

Fig. 14. Comparison of 2-NP, 3-NP and 4-NP mineralization in the visible portion of sunlight to that of complete spectrum sunlight exposure over 1% W^{6+}–ZnO. The UV portion of sunlight was blocked by using UV filter.

observed in the solution. The hindered orientation of NO_2 groups in 3-NP further lowers the rate of release of NO_2^- ions.

The quick disappearance of nitrophenol substrates and the release of NO_2^- ions in the solution predicts that $O_2^{\bullet -}$ anion radicals, being charged in nature, attack the NO_2 group attachment site to displace NO_2^- ions in the solution rather than any other activated position that leads to the ring opening. Along with the other finding, the absence of aromatic intermediates, as verified by HPLC analysis and GC–MS analysis, further strengthen the proposed mode of interaction of $O_2^{\bullet -}$ anions with nitrophenols. The proposed mechanism of interaction of $O_2^{\bullet -}$ anions with 4-NP can be illustrated as below.

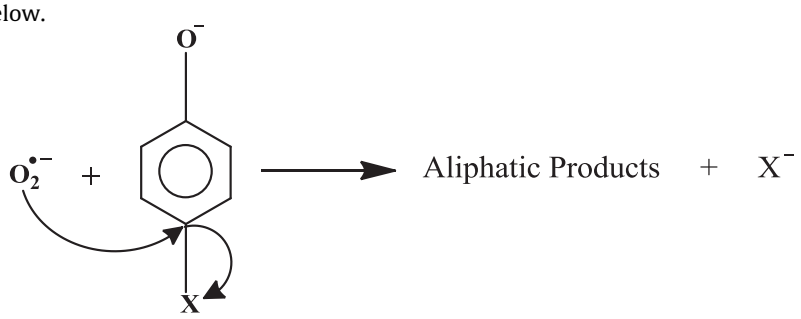

The ring opening products, intermediates that were identified by the GC–MS analysis of the selected samples were aliphatic alcohols, aldehydes an carboxylic acid. Some of the structures identified by the library search of the equipment are mentioned below.

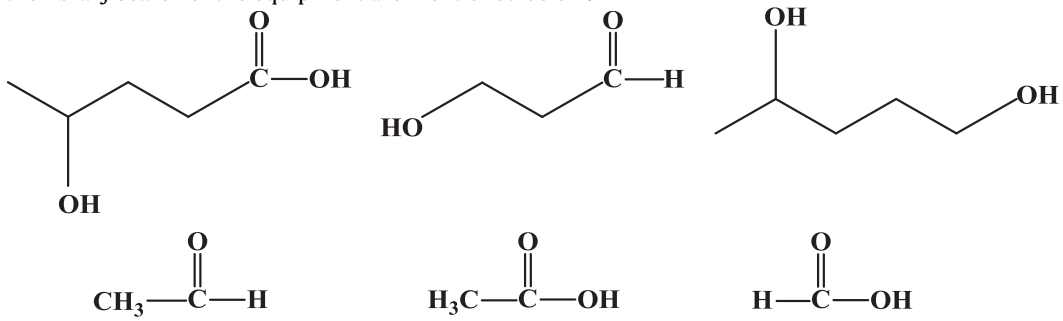

It is important to mention here there in the presence of the variety of the reactions occurring simultaneously that is the characteristic of photocatalysed reactions it is hard to propose the exact mechanism of nitrophenol degradation however, based on the experimental evidences and instrumental analysis the process of degradation can be speculated.

The comparison of the results obtained by HPLC, TOC, IC and GC–MS analysis can be summarized as:

- The mineralization process proceeds through the formation of intermediates.
- Unlike $OH^{\bullet}$ degradation, the intermediates were found aliphatic oxygenates.
- The superoxide anion radicals are non-selective in attack and degrade the nitrophenol isomers and intermediates simultaneously.
- The attack of superoxide anion radicals on NO_2 bearing carbon leads to the release of nitrite ions in the solution as well as ring opening producing aliphatic oxygenates.
- NO_2^- ions are gradually oxidized further to NO_3^- ions.

The activity of 1% W^{6+}–ZnO in the visible segment of the solar spectrum i.e. 400–800 nm, was evaluated by performing the experiments for the degradation of 2-NP, 3-NP and 4-NP by using Pyrex glass UV cutoff filter. The absorption spectrum of the filter is given in Fig. S8 (supplementary details). The comparison of degradation profiles of the three isomers is presented in Fig. 14a–c, where in the visible portion of the sunlight, compared to complete solar spectrum, a 15–20% decrease in the overall degradation of the three isomers can be observed. Compared to complete solar spectrum, the complete degradation of 2- and 4-NP in visible portion was delayed by 30 min. The same effect was observed for 3-NP. It is important to mention here that no noticeable change was observed in the by-products, illustrating that identical oxidizing species are produced in visible portion as well as in complete sunlight exposure. However, with the exclusion of energetic UV radiations required to excite ZnO (E_g = 3.1 eV), the production of oxidizing species, mainly $O_2^{\bullet -}$ anions, is affected that leads to a moderate decrease in the photocatalytic activity. ZnO failed to exhibit any noticeable activity in the visible region of the solar spectrum.

The effect of the increasing density of W^{6+} states at the surface of ZnO was evaluated by performing the sunlight photocatalytic experiments for the degradation of nitrophenol isomers with 5% W^{6+}–ZnO, 10% W^{6+}–ZnO and 15% W^{6+}–ZnO photocatalysts and results were compared with that of 1% W^{6+}–ZnO. Noticeably, the activity of all the impregnated catalysts was much higher than pure ZnO. The comparison of percentage degradation of 2-NP over W^{6+} impregnated ZnO photocatalysts is presented in Fig. 15, where it can be noticed that up to 5% W^{6+} loading, the degradation activity remains consistent. The further increase in W^{6+} metal loading causes a significant decrease in the activity. A similar trend was observed for the degradation of 3- and 4-NP. The increased presence of intermediates for 5% and 10% W^{6+} loading was also observed. The identification of hydroxylated aromatic products, although in very low concentration, revealed that the increased W^{6+} loading promotes the yield of hydroxyl radicals. The layer by layer deposition of W^{6+} ions results in the formation of surface WO_3 that although enhance the absorption of photons in the visible region (Figs. 1 and 2) and significantly suppress recombination of charge carriers (Fig. 3) but looses the ability to transfer the photogenerated electrons to oxygen that results in the decrease of photocatalytic degradation.

The effect of repeated exposure to the activity of same catalyst was studied by exposing a fixed amount of 1% W^{6+}–ZnO for the degradation of 2-NP for a period of 60 min each week for four weeks.

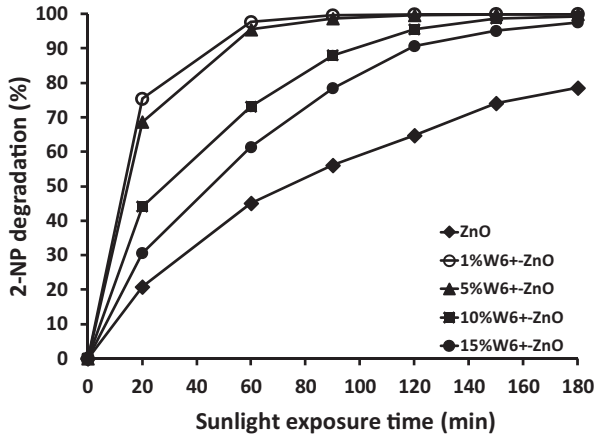

Fig. 15. Effect of increasing W^{6+} loading on the degradation of 2-NP.

No noticeable change in activity or deactivation of the catalyst was observed. The photocorrosion of the pure and W^{6+} impregnated ZnO catalysts were monitored by ICP-OES analysis for the sunlight exposed samples at regular interval. No release of Zn^{2+} was observed for pure and W^{6+} impregnated ZnO catalysts, which led to the conclusion that under mild exposure conditions (~3–5% UV) like natural sunlight, ZnO do not undergo photocorrosion however, under intense UV exposure (simulated sunlight generated by lamps or pure UV exposure), the situation may be different.

4. Conclusions

The impregnation by W^{6+} improves the spectral response of ZnO in the visible region and suppresses the undesired charge carrier recombination process without affecting the morphology. The surface presence of W^{6+} states promotes the capture and delivery of photogenerated electrons to dissolved/adsorbed oxygen to form superoxide anion radicals. The photocatalytic degradation process proceeds through the interaction of superoxide ions with nitrophenol substrates and formation of aliphatic intermediates. The aliphatic intermediates are further interacted by superoxide ions for complete mineralization. Being charged in nature, superoxide anions are selective in interaction with the nitrophenol isomers. The extent of interaction between the superoxide anion radicals depends upon the chemical structure, stability and position of the NO_2 group. The study has proved the practical applicability of aqueous photocatalysis for the removal of hazardous stable contaminants in the sunlight exposure without leaving any toxic by-products.

Acknowledgements

Iqbal M.I. Ismail, A. Hameed and M. Aslam are thankful to CEES, KAU (Project No. 2/W/1435) and Ministry of Higher Education, KSA, for support. M.A. Gondal is thankful to KFUPM for the support through project # MIT-11109,11110.

Appendix A. Supplementary data

Supplementary material related to this article can be found, in the online version, at http://dx.doi.org/10.1016/j.apcatb.2014.05.023.

References

[1] U.S. Environmental Protection Agency, Ambient Water Quality Criteria for Nitrophenols, 1980, Washington, DC.
[2] S.S. Adav, M.Y. Chen, D.J. Lee, N.Q. Ren, Chemosphere 67 (2007) 1566–1572.
[3] N. Calace, E. Nardi, B.M. Petronio, M. Pietroletti, Environ. Pollut. 118 (2002) 315–319.
[4] F.A. Carey, Organic Chemistry, 4th ed., McGraw-Hill, New York, 2000, pp. 945.
[5] O.A. O'Connor, L.Y. Young, Environ. Toxicol. Chem. 8 (1989) 853–862.
[6] M.N. Chong, B. Jin, C.W.K. Chow, C. Saint, Water Res. 44 (2010) 2997–3027.
[7] M. Akcay, M. Akcay, J. Hazard. Mater. B113 (2004) 189–193.
[8] E. Marais, T. Nyokong, J. Hazard. Mater. 152 (2008) 293–301.
[9] Y. Ku, K.C. Lee, J. Hazard. Mater. B80 (2000) 59–68.
[10] Z. Aksu, J. Yener, Waste Manage. 21 (2001) 695–702.
[11] A. Mills, S. Le Hunte, J. Photochem. Photobiol. A 108 (1997) 1–35.
[12] D.F. Ollis, E. Pelizzetti, N. Serpone, Environ. Sci. Technol. 25 (1991) 1522–1529.
[13] M.R. Hoffmann, S. Martin, W. Choi, D.W. Bahnemann, Chem. Rev. 95 (1995) 69–96.
[14] R. Andreozzi, V. Caprio, A. Insola, R. Marotta, Catal. Today 53 (1999) 51–59.
[15] D.A. Tryk, A. Fujishima, K. Honda, Electrochim. Acta 45 (2000) 2363–2376.
[16] M. Kositzi, I. Poulios, S. Malato, J. Caceres, A. Campos, Water Res. 38 (2004) 1147–1154.
[17] S. Malato, P. Fernández-Ibáñez, M.I. Maldonado, J. Blanco, W. Gernjak, Catal. Today 147 (2009) 1–59.
[18] Z. Ali, M. Aslam, I.M.I. Ismail, A. Hameed, S.T. Hussain, M.N. Chaudhry, M.A. Gondal, J. Environ. Sci. Health Part A 49 (2014) 1–11.
[19] D. Bahnemann, Sol. Energy 77 (2004) 445–459.
[20] B. Subash, B. Krishnakumar, V. Pandiyan, M. Swaminathan, M. Shanthi, Sep. Purif. Technol. 96 (2012) 204–213.
[21] B. Subash, B. Krishnakumar, R. Velmurugan, M. Swaminathan, M. Shanthi, Catal. Sci. Technol. 2 (2012) 2319–2326.
[22] B. Subash, B. Krishnakumar, M. Swaminathan, M. Shanthi, Langmuir 29 (2013) 939–949.
[23] B. Subash, B. Krishnakumar, R. Velumurugan, S. Balachandran, M. Swaminathan, Mater. Sci. Semicond. Process. 16 (2013) 859–867.
[24] B. Krishnakumar, R. Velumurugan, B. Subash, M. Swaminathan, Indian J. Chem. 51 (2012) 580–585.
[25] S. Rehman, R. Ullah, A.M. Butt, N.D. Gohar, J. Hazard. Mater. 170 (2009) 560–569.
[26] B. Krishnakumar, M. Swaminathan, Spectrochim. Acta A 81 (2011) 739–744.
[27] B. Krishnakumar, K. Selvam, R. Velmurugan, M. Swaminathan, Desalin. Water Treat. 24 (2010) 132–139.
[28] S. Chakrabarti, B.K. Dutta, J. Hazard. Mater. B112 (2004) 269–327.
[29] J.N. Daneshvar, D. Salari, A.R. Khataee, J. Photochem. Photobiol. A: Chem. 162 (2004) 317–322.
[30] S.K. Kansal, A.H. Ali, S. Kapoor, Desalination 259 (2010) 147–155.
[31] R. Velmurugan, M. Swaminathan, Sol. Energy Mater. Sol. Cells 95 (2011) 942–950.
[32] T.Y. Leung, C.Y. Chan, C. Hu, J.C. Yu, P.K. Wong, Water Res. 42 (2008) 4827–4837.
[33] M. Miyauchi, A. Nakajima, T. Watanabe, k. Hashimoto, Chem. Mater. 14 (2002) 2812–2816.
[34] Ü. Özgür, Ya.I. Alivov, C. Liu, A.B. Teke, M.A. Reshchikov, S. Doğan, V. Avrutin, S.-J. Cho, H. Morkoç, J. Appl. Phys. 98 (2005), 041301-1-103.
[35] A. Mclaren, T. Valdes-Solis, G. Li, S.C. Tsang, J. Am. Chem. Soc. 131 (2009) 12540–12541.
[36] C. Yu, K. Yang, Y. Xie, Q. Fan, J.C. Yu, Q. Shu, C. Wanga, Nanoscale 5 (2013) 2142–2151.
[37] B. Subash, B. Krishnakumar, M. Swaminathan, M. Shanthi, J. Mol. Catal. A 366 (2013) 54–63.
[38] A. Hameed, I.M.I. Ismail, M. Aslam, M.A. Gondal, Appl. Catal. A: Gen. 470 (2014) 327–335.
[39] L. Palmisano, A. Sclafani, Heterogeneous photocatalysis, in: M. Schiavello (Ed.), Photoscience and Photoengineering, vol. 3, John Wiley & Sons, Chichester, 1997, p. 109 (Chapter 4).
[40] J. Soria, J.C. Conesa, V. Augugliaro, L. Palmisano, M. Schiavello, A. Sclafani, J. Phys. Chem. 95 (1991) 274–282.
[41] N. Serpone, E. Pelizzetti, Photocatalysis: Fundamentals and Applications, Wiley, New York, 1989.
[42] M. Schiavello, Photocatalysis and Environment: Trends and Applications, Kluwer Academic Publishers, Dordrecht, The Netherlands, 1988.
[43] S.M. Lam, J.C. Sin, I. Satoshi, A.Z. Abdullah, A.R. Mohamed, Appl. Catal. A: Gen. 471 (2014) 126–135.
[44] J.C. Sin, S.M. Lam, K.T. Lee, A.R. Mohamed, Mater. Sci. Semicond. Process. 16 (2013) 1542–1550.
[45] B. Subash, B. Krishnakumar, B. Sreedhar, M. Swaminathan, M. Shanthi, Superlattices Microstruct. 54 (2013) 155–171.
[46] A. Di Paola, V. Augugliaro, L. Palmisano, G. Pantaleo, E. Savinov, J. Photochem. Photobiol. A: Chem. 155 (2003) 207–214.
[47] A. Di Paola, G. Marcì, L. Palmisano, M. Schiavello, K. Uosaki, S. Ikeda, B. Ohtani, J. Phys. Chem. B 106 (2002) 637–645.
[48] S. Lathasree, A. Nageswara Rao, B. Siva Sankar, V. Sadasivam, K. Rengaraj, J. Mol. Catal. A 223 (2004) 101–105.
[49] S. Ahmed, M.G. Rasul, W.N. Martens, R.J. Brown, M.A. Hashib, Desalination 261 (2010) 3–18.
[50] W. Bahnemann, M. Muneer, M.M. Haque, Catal. Today 124 (2007) 133–148.
[51] S.K. Pardeshi, A.B. Patil, Sol. Energy 82 (2008) 700–705.
[52] D. Chen, A.K. Ray, Water Res. 32 (1998) 3223–3234.
[53] M. Sugiyama, Z. Salehi, M. Tokumura, Y. Kawase, Water Sci. Technol. 65 (2012) 1882–1886.
[54] V. Augugliaro, M.J. López-Muños, L. Palmisano, J. Soria, Appl. Catal. A 101 (1993) 7–13.

[55] N. San, A. Hatipoglu, G. Kocturk, Z. Cinar, J. Photochem. Photobiol. A 146 (2002) 189.
[56] U.I. Gaya, A.H. Abdullah, Z. Zainal, M.Z. Hussein, Int. J. Chem. 2 (2010) 180–189.
[57] V. Augugliaro, L. Palmisano, M. Schiavello, A. Sclafani, Appl. Catal. 69 (1991) 323–340.
[58] B. Zhao, G. Mele, I. Pio, J. Li, L. Palmisano, G. Vasapollo, J. Hazard. Mater. 176 (2010) 569–574.
[59] A. Hameed, M.A. Gondal, Z.H. Yamani, Catal. Commun. 5 (2004) 715–719.
[60] V. Srikant, D.R. Clarke, J. Appl. Phys. 83 (1998) 5447–5451.
[61] M. Willander, O. Nur, J.R. Sadaf, M.I. Qadir, S. Zaman, A. Zainelabdin, N. Bano, I. Hussain, Materials 3 (2010) 2643–2667.
[62] A.G. Joshi, S. Sahai, N. Gandhi, Y.G. Radha Krishna, D. Haranatha, Appl. Phys. Lett. 96 (2010) 123102–123103.
[63] T.H. Pan, W.I. Lee, Chem. Mater. 18 (2006) 847–853.
[64] C.S. Turchi, D.F. Ollis, J. Catal. 122 (1990) 178–192.
[65] P. Pichat, Photocatalysis and Water Purification from Fundamentals to Recent Applications, first ed., Wiley-VCH Verlag GmbH & Co. KGaA, 2013.
[66] M.A. Henderson, Surf. Sci. Rep. 66 (2011) 185–297.
[67] B.H.J. Bielski, D.E. Cabelli, R.L. Arudi, J. Phys. Chem. Ref. Data 14 (1985) 1041–1100.